

# Supplement of Locally emitted fungal spores serve as high temperature ice nucleating particles in the European sub-Arctic

Jürgen Gratzl<sup>1</sup>, Alexander Böhmmländer<sup>2</sup>, Sanna Pätsi<sup>3</sup>, Clara-E. Pogner<sup>4</sup>, Markus Gorfer<sup>4</sup>, David Brus<sup>5</sup>, Konstantinos Matthaios Doulgeris<sup>5</sup>, Florian Wieland<sup>1</sup>, Eija Asmi<sup>5</sup>, Annika Saarto<sup>3</sup>, Ottmar Möhler<sup>2</sup>, Dominik Stolzenburg<sup>1</sup>, and Hinrich Grothe<sup>1</sup>

<sup>1</sup>Institute of Materials Chemistry, TU Wien, Vienna, 1060, Austria

<sup>2</sup>Institute of Meteorology and Climate Research, Atmospheric Aerosol Research (IMK-AAF), Karlsruhe Institute of Technology (KIT), Karlsruhe, 76121, Germany

<sup>3</sup>Biodiversity Unit, University of Turku, Turku, Finland

<sup>4</sup>Center for Health and Bioresources, AIT Austrian Institute of Technology GmbH, Tulln, 3430, Austria

<sup>5</sup>Finnish Meteorological Institute, Atmospheric Composition Research, Helsinki, FI-00101, Finland

**Correspondence:** Hinrich Grothe (hinrich.grothe@tuwien.ac.at)

## 1 Comparison of WIBS and APS

An Aerodynamic Particle Sizer (TSI, USA) APS was operated alongside WIBS to compare particle concentrations and validate WIBS data. The APS measures particles with an aerodynamic diameter  $>0.523$   $\mu\text{m}$ . 30 min mean values of APS data and Total Aerosol Particles (TAPs) from WIBS were calculated and compared during the PaCE22 campaign. APS concentrations were on average 3 times higher than those recorded by WIBS. The aerodynamic diameter tends to be larger than the optical equivalent diameter. Consequently, APS may have detected smaller particles than WIBS. A scatter plot can be seen in fig S1.

## 2 A closer look on the other HFAP types

Figure S2, presents daily mean concentrations of TAPs, highly fluorescent aerosol particles (HFAPs) and all types of HFAPs, alongside temperature and snow depth, both measured at Kenttäröva research station (N67°59.237', E24°14.579') inside the forest near Sammaltunturi. Seasons were defined based on daily mean temperatures: autumn ( $< 10$  °C), winter (mostly  $< 0$  °C), spring (mostly between  $0$  °C and  $10$  °C) and summer (mostly over  $10$  °C). Winter started three days before permanent snow cover and ended 3 days after snow melt began. The polar night started on December 21. Spring included most of the snow melt period and extended 17 days into the snow-free period. Median values, 25th and 75th percentiles and fractions of TAPs and all HFAP types together with meteorological parameter for the four seasons are summarized in tab. S1.

A seasonal trend is apparent for A particles (Fig. S2 (c)), with the highest median concentration in summer ( $2.2 \times 10^{-3}$   $\text{cm}^{-3}$ ). However, notable peaks also occurred in winter. Figure S4 (e) shows, that many daily mean size distributions during the snow covered period showed higher concentrations for particles  $< 1$   $\mu\text{m}$  than during the snow free period, while larger particles dominated during warmer periods. For instance, the day of maximum concentration coincided with the maximum of

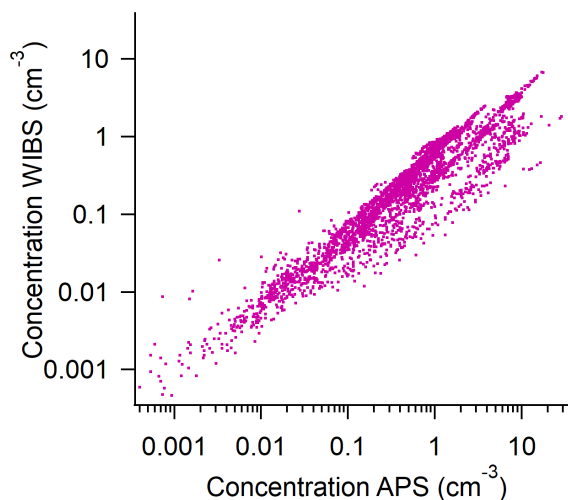


**Figure S1.** Scatter plot of TAP concentrations measured with WIBS vs. concentrations of particles with aerodynamic diameter > 523 nm measured with APS with 30 min resolution.

TAPs during winter, on December 11th (labeled (2) in Fig. S2 (a)). On this day, air masses originated from Western Russia, suggesting long-range transport. Size distributions indicate that both A particles and HFAPs were smaller compared to peak days in other seasons. As the arriving air masses went over industrialized areas, this suggests a possible anthropogenic origin. A more detailed description of this event can be read in sect. 3.2. Summer diurnal trends (Fig. S3) show that A particles and ambient temperature both underwent a very similar trend over the day. In chamber experiments, bacteria have been classified almost exclusively as A particles (Savage et al., 2017; Hernandez et al., 2016), although field studies have not confirmed this correlation. Previous research (Lighthart and Shaffer, 1995; Abdel Hameed et al., 2009) observed afternoon accumulation peaks for airborne bacteria, indicating a possible connection between ambient temperature and the emission of bacteria. Diesel soot, also tested by Savage et al. (2017), fluoresces in the A channel as well, implying that A particles here likely included both anthropogenic aerosols and bacteria, with anthropogenic influence being stronger in winter. The concentration of bacteria over vegetated surfaces (close to forested ground and high alpine) was estimated to be  $\approx 10^4 \text{ m}^{-3}$  (Healy et al., 2014; Bauer et al., 2002; Burrows et al., 2009; Després et al., 2012). This is one order of magnitude greater than the concentration of A particles measured here.

B and BC particles (Fig. S2 (d)) showed similar behavior, both correlating strongly with TAPs (Pearson  $r = 0.66$  for B particles and  $0.52$  for BC particles,  $p < 0.0001$ ). While BC particles lacked a clear seasonal cycle, their concentration appears suppressed by snow cover from October to December 2022, resulting in the lowest median levels in winter ( $3.6 \times 10^{-4} \text{ cm}^{-3}$ ). The highest concentration of BC particles was in summer with  $2.3 \times 10^{-3} \text{ cm}^{-3}$ . The median concentration of B particles was the most consistent over the seasons with lowest in winter ( $1.3 \times 10^{-4} \text{ cm}^{-3}$ ) and highest in summer ( $4.0 \times 10^{-3} \text{ cm}^{-3}$ ). From April 2023 onward, BC concentration trends closely followed B particles, with three prominent springtime peaks (labeled

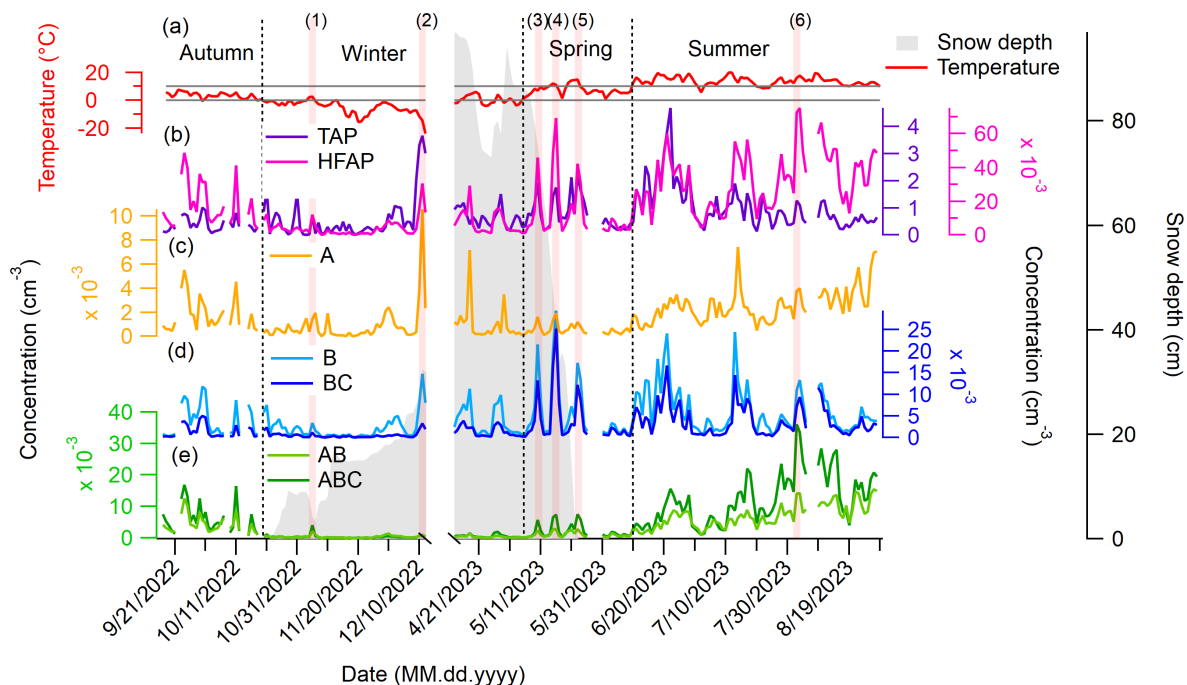


**Figure S2.** Daily mean concentrations of TAPs, HFAPs and all fluorescent particle types, mean snow depth and ambient temperature inside a near spruce forest. (a) Temperature measured at Kenttäröva station is used to define the meteorological seasons. (b) TAPS and HFAPs, (c) A particles, (d) B and BC particles, (e) AB and ABC particles. Horizontal transparent red lines are labeled with a number and mark certain days discussed in the text.

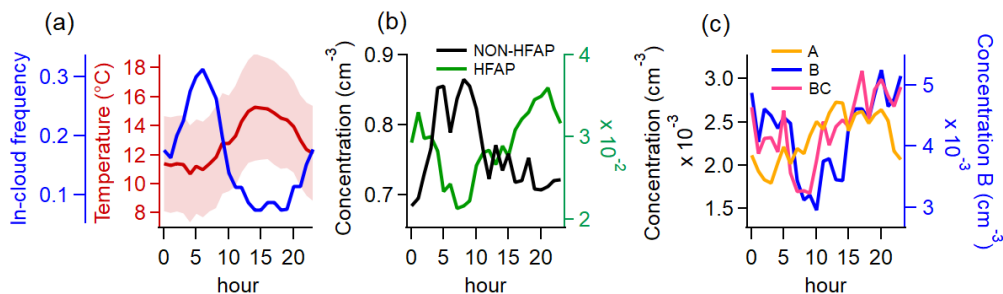


**Figure S3.** Diurnal cycle of summertime meteorology and fluorescent aerosol. (a) In cloud frequency and median temperature. (b) Median NON-HFAPs and HFAP concentrations. (c) Median A, B and BC particle concentrations

(3), (4), and (5) in Fig. S2 (a)). On days (4) and (5), air masses spend most of the prior three days over the gulf of Bothnia, or its eastern coastline, suggesting a possible coastal inversion, from where enriched anthropogenic aerosol could have been transported to Pallas. These peaks also aligned with elevated eBC concentrations. A detailed description of these events can be

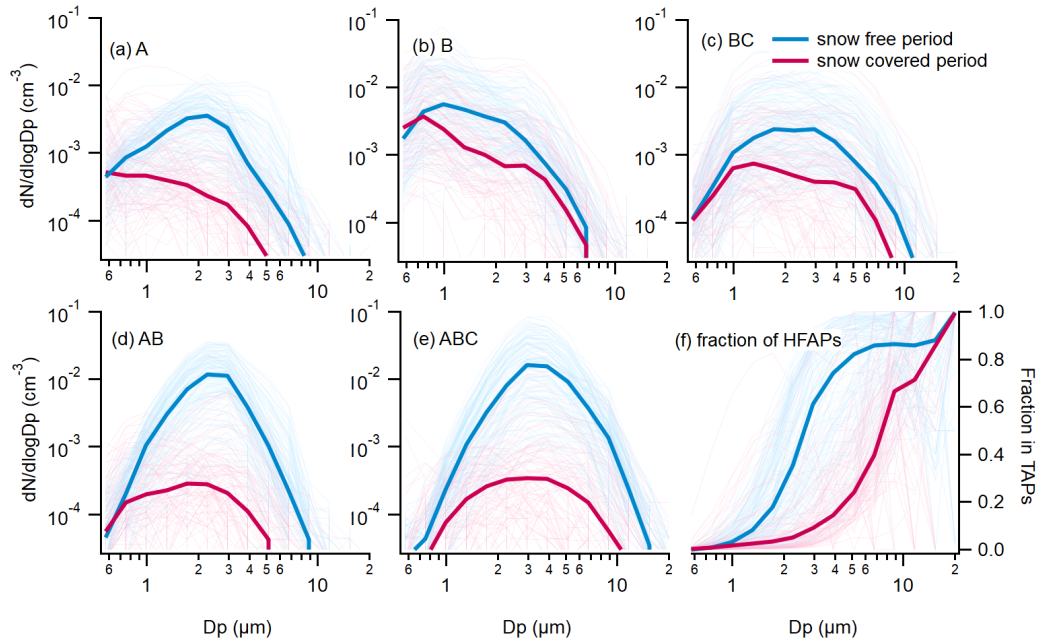


**Figure S4.** (a)-(g): Size distributions of all particles types measured with WIBS. (h) Fraction of HFAPs per particles size. Thick blue lines: Median distributions during snow free periods. Soft blue lines: Daily mean distributions during snow free periods. Thick red lines: Median distributions during snow covered period. Soft red lines: Daily mean distributions during snow covered period.

seen in sect. 3.3. B and BC particles, although likely heavily influenced by anthropogenic sources due to their high correlation with eBC mass concentration (see Sect. 3.4 in the main text), followed the summertime diurnal trend of all HFAPs (Fig.S3), suggesting local anthropogenic emissions, rather than far range transported ones were important for this signal. Biomass burning from local or regional population and vehicle exhaustion may contribute to their presence.

### 45 3 Case studies

#### 3.1 November 5, 2022: Temporary snow melt

Permanent snow cover significantly reduced HFAP concentrations, particularly AB and ABC particles. On November 5, 2022, a brief melting period coincided with a sharp increase in AB and ABC particles. To determine whether this rise was caused by snow melt or a shift in air mass direction, we calculated 72 h back trajectories for this day as well as the day before and after  
 50 (Fig.S5 (a)). Since no major change in air mass direction occurred, local meteorological conditions were likely responsible. In Fig.S5 (b), size distributions of ABC particles show a strong increase in  $\approx 3 \mu\text{m}$  particles around 6 am UTC on November 5. Snow depth (measured at 6 am UTC) in Pallas, indicates that melting began two days earlier. In Kolari only 70 km south of



**Table S1.** Median concentration values and percentiles (25th and 75th) of TAPs, HFAPs and particles types for every season and meteorological parameters. All concentration values are reported in  $\text{std cm}^{-3}$ .

Season	Autumn	Winter	Spring	Summer
Dates	Sept 17 2022- Oct 17 2022	Oct 18 2022- Dec 12 2022, April 13 2023- May 5 2023	May 5 2023- June 9 2023	June 10 2023- Aug 28 2023
hours of data	287	1727	658	1743
Median TAP	$2.8 \times 10^{-1}$	$3.3 \times 10^{-1}$	$4.4 \times 10^{-1}$	$7.5 \times 10^{-1}$
Percentiles TAP	$1.2 \times 10^{-1}$ ; $6.2 \times 10^{-1}$	$8.2 \times 10^{-2}$ ; $8.8 \times 10^{-1}$	$2.5 \times 10^{-1}$ ; 1.2	$4.5 \times 10^{-1}$ ; 1.4
Median HFAP	$1.2 \times 10^{-2}$	$2.9 \times 10^{-3}$	$5.4 \times 10^{-3}$	$3.0 \times 10^{-2}$
Percentiles HFAP	$5.81 \times 10^{-3}$ ; $2.83 \times 10^{-2}$	$1.2 \times 10^{-3}$ ; $6.8 \times 10^{-3}$	$2.9 \times 10^{-3}$ ; $1.4 \times 10^{-2}$	$1.5 \times 10^{-2}$ ; $4.5 \times 10^{-2}$
Median fraction HFAP	$5.6 \times 10^{-2}$	$1.0 \times 10^{-2}$	$1.4 \times 10^{-2}$	$3.5 \times 10^{-2}$
Percentiles of fraction	$3.4 \times 10^{-2}$ ; $8.8 \times 10^{-2}$	$4.9 \times 10^{-3}$ ; $2.0 \times 10^{-2}$	$6.7 \times 10^{-3}$ ; $2.6 \times 10^{-2}$	$1.7 \times 10^{-2}$ ; $7.0 \times 10^{-2}$
Median A	$1.2 \times 10^{-3}$	$3.7 \times 10^{-4}$	$3.7 \times 10^{-4}$	$2.2 \times 10^{-3}$
Percentiles A	$5.5 \times 10^{-4}$ ; $2.9 \times 10^{-3}$	$1.3 \times 10^{-4}$ ; $9.9 \times 10^{-4}$	$1.8 \times 10^{-4}$ ; $7.3 \times 10^{-4}$	$1.3 \times 10^{-3}$ ; $3.4 \times 10^{-3}$
Median B	$1.96 \times 10^{-3}$	$1.25 \times 10^{-3}$	$1.94 \times 10^{-3}$	$4.0 \times 10^{-3}$
Percentiles B	$6.7 \times 10^{-4}$ ; $6.7 \times 10^{-3}$	$5.4 \times 10^{-4}$ ; $3.6 \times 10^{-3}$	$9.1 \times 10^{-4}$ ; $5.9 \times 10^{-3}$	$2.0 \times 10^{-3}$ ; $8.6 \times 10^{-3}$
Median BC	$5.8 \times 10^{-4}$	$3.6 \times 10^{-4}$	$1.02 \times 10^{-3}$	$2.34 \times 10^{-3}$
Percentiles BC	$2.4 \times 10^{-4}$ ; $2.6 \times 10^{-3}$	$1.2 \times 10^{-4}$ ; $9.0 \times 10^{-4}$	$4.2 \times 10^{-4}$ ; $3.1 \times 10^{-3}$	$9.4 \times 10^{-4}$ ; $5.0 \times 10^{-3}$
Median AB	$3.1 \times 10^{-3}$	$1.9 \times 10^{-4}$	$6.0 \times 10^{-4}$	$5.8 \times 10^{-3}$
Percentiles AB	$1.7 \times 10^{-3}$ ; $6.3 \times 10^{-3}$	$6.1 \times 10^{-5}$ ; $4.7 \times 10^{-4}$	$2.5 \times 10^{-4}$ ; $3.1 \times 10^{-3}$	$3.0 \times 10^{-3}$ ; $9.7 \times 10^{-3}$
Median ABC	$4.4 \times 10^{-3}$	$1.9 \times 10^{-4}$	$9.0 \times 10^{-4}$	$9.5 \times 10^{-3}$
Percentiles ABC	$1.9 \times 10^{-3}$ ; $8.8 \times 10^{-2}$	$6.1E \times 10^{-5}$ ; $4.4 \times 10^{-4}$	$4.3 \times 10^{-4}$ ; $2.2 \times 10^{-3}$	$4.3 \times 10^{-3}$ ; $1.8 \times 10^{-2}$
Median temperature ( $^{\circ}\text{C}$ )	2.7	-3.4	5.1	12.4
Percentiles temperature	0.9;4.2	-6;-1.2	2.5;8.1	10.1;15.1
Median wind speed ( $\text{ms}^{-1}$ )	6.8	6.8	6.5	5.3
percentiles wind speed	4.9;8.3	4.8;9	4.8;8.4	3.8;7.3
Percentage in cloud (%)	39	43	6	16

Pallas, snow has completely melted by 6 am UTC on November 5. This suggests that biological activity increased immediately after snow melt, with air masses transporting biological particles from the snow-free biosphere south of Pallas.

## 55 3.2 December 11, 2022: Peak A concentration

On December 11, 2022, the highest A concentrations and elevated TAP levels were recorded. On this day, air masses primarily arrived from Western Russia (Fig. S6 (a)), passing over the Central Economic Region, a highly industrialized area. Figure S6 (b) shows, that while both A and TAP concentrations rose, the increase was not simultaneous. However  $\text{NO}_x$  and  $\text{SO}_2$  levels increased concurrently with A particles. Therefore, air, polluted with these trace gasses also carried A particles, suggesting, that A particles arriving at the station were anthropogenic in origin, rather than biological.



### 3.3 May 7 - 25, 2023: Peak B and BC concentrations

Three distinct peaks in B and BC concentrations occurred in May 2023, around the 10th, 16th and 24th. Back trajectories show that during the latter two peaks, air masses remained close to the surface over the Gulf of Bothnia for three days before arriving at the station (Fig. S7 (b) and (c)). A likely cause is a coastal inversion, which trapped pollutants and led to a sharp rise in B and BC particle concentrations. Figure S7 (d) displays B and BC particle size distributions, revealing a simultaneous increase in both types. B particles dominated below 1  $\mu\text{m}$ , while BC particles were mostly > 2  $\mu\text{m}$ . Since fluorescence intensity depends on particle size (Hill et al., 2001), it is plausible that both types share the same origin, but only larger particles exceeded the fluorescence threshold in FL3, classifying them as BC rather than B particles. During the same period, eBC mass concentration increased similarly. The strong overall correlation of B and BC concentration and eBC throughout the whole measurement period suggests that these particles largely consist of black carbon. Even during the first peak (Fig. S7(a)), when only a small fraction of air masses had passed over the Gulf of Bothnia, eBC concentrations still increased simultaneously.

### 3.4 02.08.2023: PEAK AB and ABC concentration

On the August 2, 2023 the maximum concentration of both AB and ABC particle concentrations were recorded. 72 h HYSPLIT back trajectories for this day show, that air masses arriving 100 m above ground came from the south and stayed close to the ground and therefore passed over heavily wooded terrain (Fig. S8 (a)). A comparison to air masses arriving 500 m above ground level show that they have covered a longer distance but most of them reached lower altitudes prior arrival above the station, indicating that at 500 m altitude, still regional emitted biological particles are the prominent source of AB and ABC particles.

## 4 Inside cloud and precipitation

Throughout the measurement period, the station was inside clouds 27 % of the time (autumn: 39 %, winter: 43 %, spring: 6 %, summer: 16 %). Cloud immersion reduced TAP and HFAP concentrations due to cloud and rain scavenging (Flossmann and Wobrock, 2010; Sellegri et al., 2003). However, TAP (and NON-HFAP) concentrations declined stronger, leading to a strong increase in fluorescent fraction for most in-cloud cases. Median values of concentrations, fractions and the change of both from out-of-cloud to in-cloud times are listed in Tab. S2 for the snow free period. During in-cloud periods, TAP concentrations dropped by 69 %, HFAPs by 51 %, and ABC by 34 %, resulting in a 128 % increase in HFAP fraction and a 232 % rise for ABC particles. Two exemplary periods with several transitions from cloud free to cloud covered conditions are depicted in Fig. S9: For most cloud events, HFAP concentrations rapidly decreased (logarithmic scale), while the fraction simultaneously increased. This effect was almost instantly reversed after the stations was out-of-cloud again. A similar effect was observed by Crawford et al. (2016) at the high altitude Jungfraujoch station. The authors suggested that non-fluorescent aerosols are more effectively removed through cloud condensation nuclei (CCN) activation and subsequent precipitation in mixed-phase clouds,



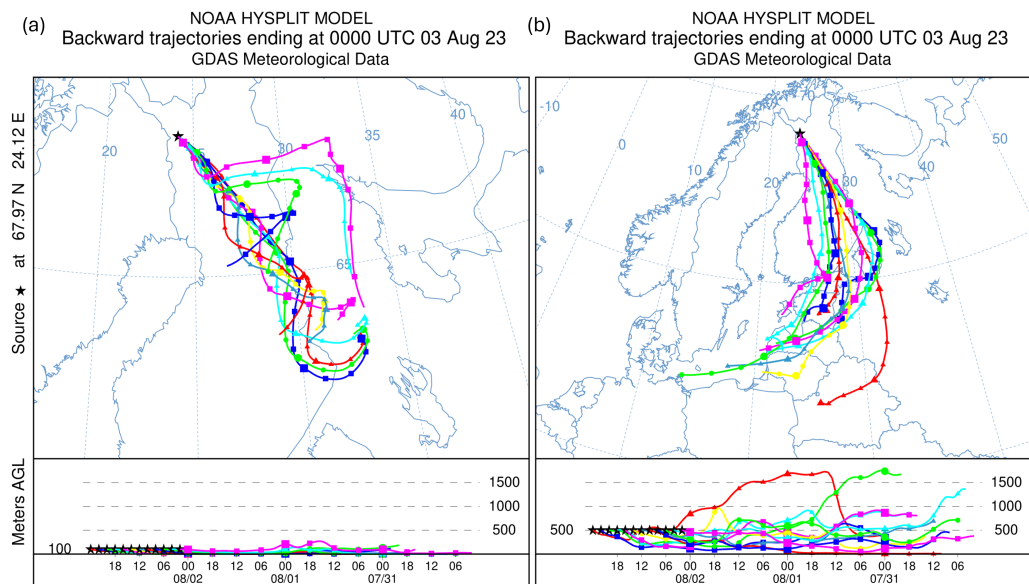


**Figure S8.** HYSPLIT back trajectories for August 2, 2023. (a) Air masses arriving 100 meters above ground level. (b) Air masses arriving 500 meters above ground level. In both cases air masses pass over the Finish boreal forest close to the ground.

**Table S2.** Median concentrations and fractions of TAPs and HFAPs for out-of-cloud and in-cloud times during the snow free period and the decrease in concentration and increase in fraction from out-of-cloud to in-cloud times.

	out of cloud		in cloud		change	
Type	median conc. ( $\text{cm}^{-3}$ )	median fr.	median conc. ( $\text{cm}^{-3}$ )	median fr.	decrease of conc. (%)	increase of fr. (%)
TAP	0.7126		0.2219		69	
HFAP	0.0251	0.0279	0.0122	0.0636	51	128
A	0.0020	0.0025	0.0008	0.0039	59	56
B	0.0038	0.0054	0.0022	0.0104	43	94
AB	0.0049	0.0057	0.0027	0.0139	46	145
BC	0.0020	0.0028	0.0009	0.0041	56	45
ABC	0.0074	0.0077	0.0049	0.0257	34	232

Multiple studies reported increases in bioaerosol concentrations during and after rain events (Rathnayake et al., 2017; Yue et al., 2016; Gosselin et al., 2016; Heo et al., 2014; Schumacher et al., 2013; Huffman et al., 2013; Prenni et al., 2013; Allitt, 2000; Hirst and Stedman, 1963; Gregory and Hirst, 1957), no such relationship was found in this study. During most rain events, the station was inside clouds, leading to the above discussed concentration decrease.

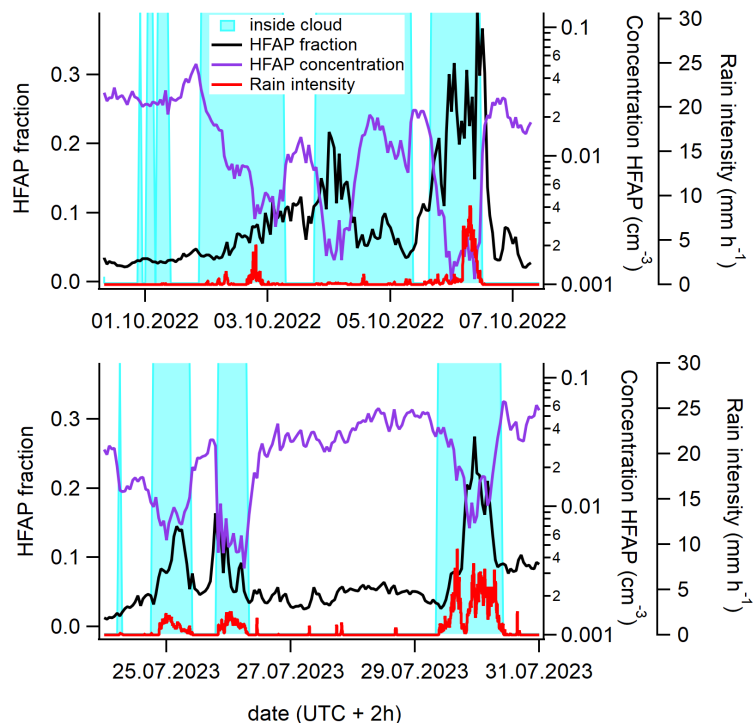


**Figure S9.** Two examples of the change of concentration and fraction of HFAPs from out-of-cloud to in-cloud transition and rain intensity.

## 5 ABC particle thresholds

For the second part of the campaign (April to September 2023) each ABC particle was analyzed individually. From all detected particles, only those exceeding the 9-sigma threshold in all three fluorescence channels (with newly measured thresholds every six hours) were classified as ABC particles. For these particles, daily mean FL1 intensity distributions were calculated by binning intensity values into 24 logarithmically equidistant channels. Figure S10(a) presents a surface plot of the intensity distributions: On the top the absolute ABC particle count in every intensity channel is described by the color scale. On the bottom the relative contribution of particle counts is plotted. This revealed 3 distinct intensity maxima, with minima between them marked as pink dashed lines in S10(a) (top). These minima were used to define new FL1 thresholds, leading to the classification of three particle subtypes: ABC\_1, ABC\_2, and ABC\_3. ABC\_1 particles have the lowest FL1 intensity with a maximum of  $7.9 \times 10^7$ . ABC\_2 possesses medium FL1 intensity that ranges between  $7.9 \times 10^7$  and  $7.0 \times 10^8$ . ABC\_3 show the highest intensity with a threshold of  $1.0 \times 10^9$ . Daily mean concentrations of these new particle types are shown in Fig. S10 (b). All three types show different temporal behavior. ABC\_2 concentrations remain near zero until the end of June and increase until early August. ABC\_3 concentrations peak at the end of June, remain low afterwards and are close to zero from mid July onward. This low concentration after mid July probably comes from the upper tail of ABC\_2 intensity distribution,

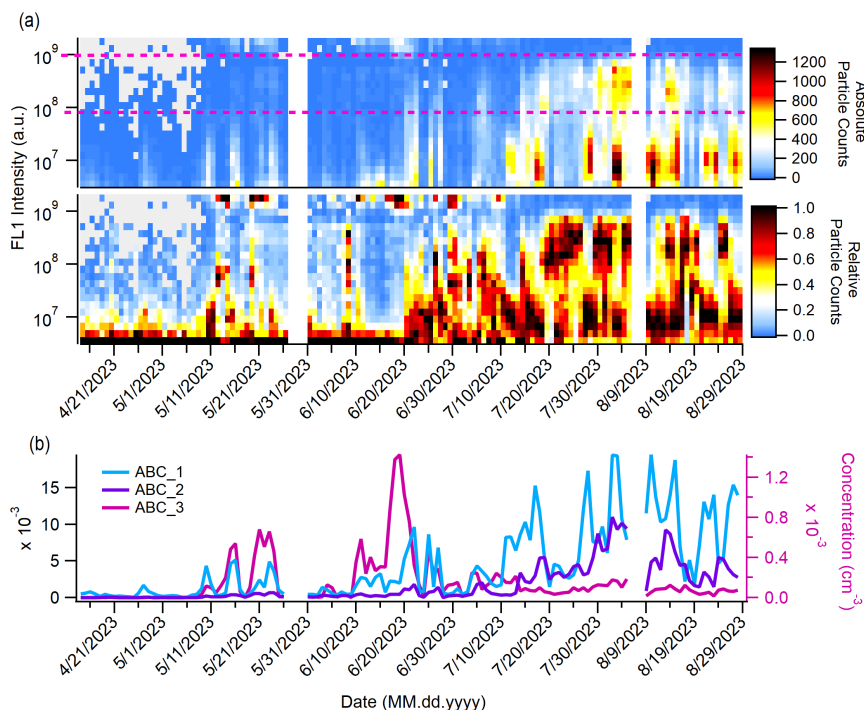


**Figure S10.** FL1 Intensity distribution for the definition of new fluorescence thresholds of ABC particles. (a) top: Evolution of daily mean particle counts in logarithmic equidistant intensity channels. Pink dashed lines indicate the upper threshold for ABC\_1 and the lower threshold for ABC\_2 at  $7.9 \times 10^7$  and the lower threshold for ABC\_3 at  $1.0 \times 10^9$ . (a) bottom: Same as top, but normalized to a total particle count of 1 for each day. (b): Daily mean concentrations for ABC\_1, ABC\_2 and ABC\_3 calculated from the new thresholds.

as the fluorescence intensity maximum shifts away from the highest intensity channel (see S10 (a) bottom). Section 3.6 of the main text demonstrates that ABC\_3 particles correlate with pollen grains. Interestingly, ABC\_1 and ABC\_2 did not exhibit stronger correlations with fungal spore counts or INP concentrations when analyzed separately, compared to their combined sum.

## 115 6 Microscopy picture of fungal spores

Figure S11 shows a microscopic picture of a Burkard slide from August 28, at 06:00 (UTC+3). Black Arrows point to particles that were reliably identified as fungal spores. Pink arrows point to particles that were believed to be fungal spores, but the identification was slightly uncertain. The yellow arrow points to a cluster of fungal spores and other particles. Please mind, that the picture only represents one focal plane, whereas during the identification, the focus was changed in order to identify a  
120 particle as a fungal spore.



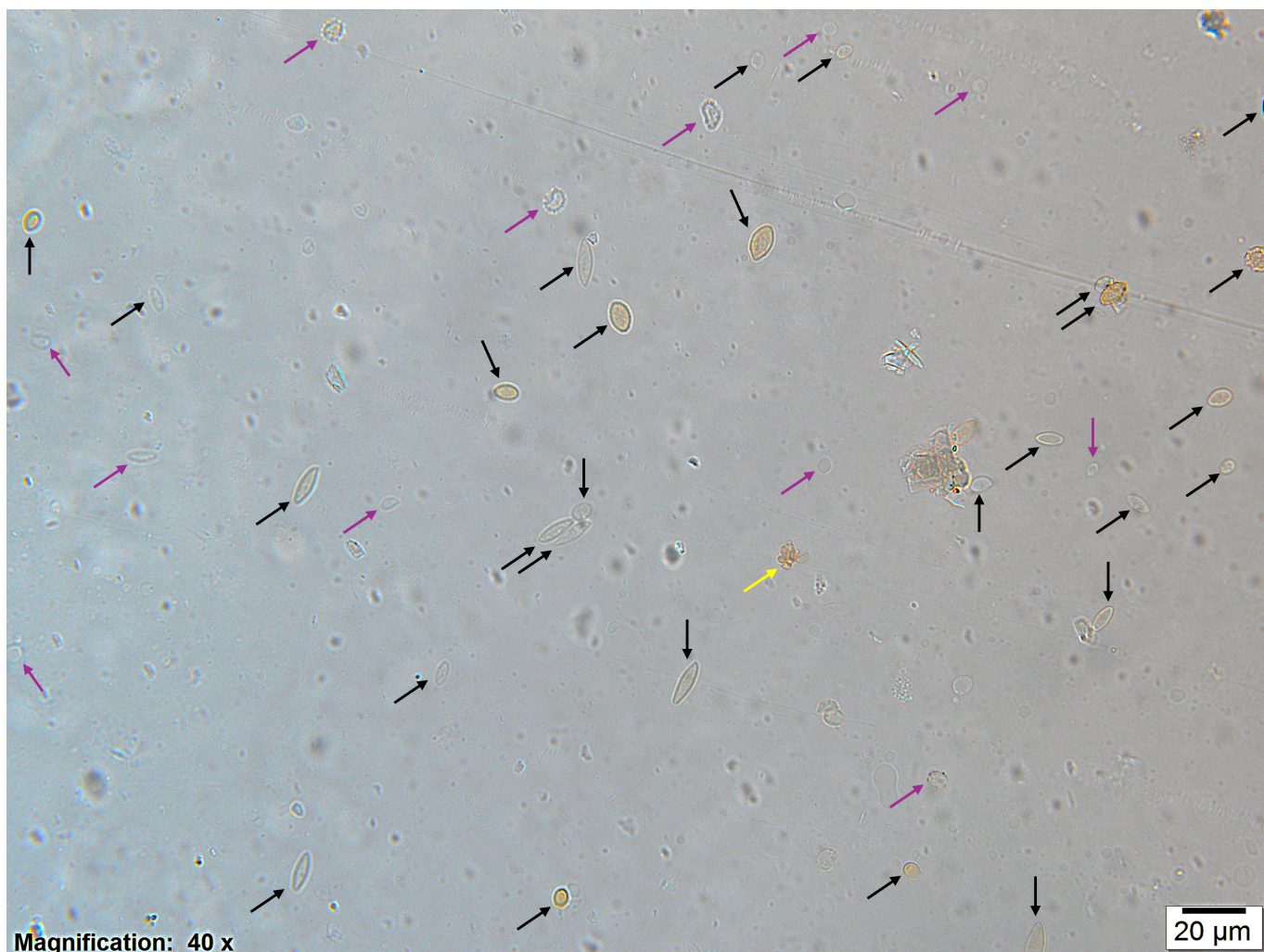


**Figure S11.** An example of fungal spore counts from August 28, 2023, 6 am (UTC+3). Black arrows point to reliable identified fungal spores, pink arrows point to particles that are probably fungal spores and the yellow arrow points to a cluster of fungal spores and other particles.

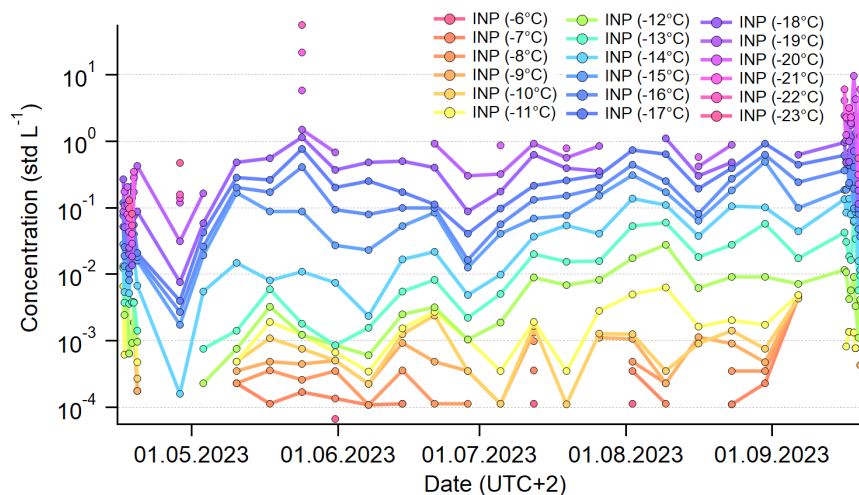
## 7 INP measurements

Figure S12 shows Ice nucleation particle (INP) concentrations active between  $-6^{\circ}\text{C}$  and  $-23^{\circ}\text{C}$ , measured using filters and analyzed with INSEKT. Figure S13 presents INP concentrations active between  $-23^{\circ}\text{C}$  and  $-31^{\circ}\text{C}$ , obtained with PINE and averaged to 1 h intervals. The PINE instrument can either measure INP concentrations at a fixed temperature over an extended period, or it scans a temperature range to record INP activity across multiple temperatures within a shorter time frame. As a result, some periods contain data for all temperatures, while others report only one. Table S3 summarizes Pearson correlation coefficients and corresponding p-values for the relation between WIBS particle concentrations and INP concentrations including only statistically significant correlations ( $p < 0.05$ ).



		INPs active above resolution															
			-9 °C	-10 °C	-11 °C	-12 °C	-13 °C	-14 °C	-15 °C	-16 °C	-17 °C	-18 °C	-23 °C	-25 °C)	-27 °C	-29 °C	-31 °C
TAP	Pearson r	1 week	0.58	1 week	1 week	1 week	1 week	1 week	1 week	1 week	1 week	1 week	1 week	1 hour	1 hour	1 hour	1 hour
	p-value		*											**	*	**	**
HFAP	Pearson r	1 week	0.64	0.60	0.81	0.80	0.84	0.82	0.81	0.56	0.52	0.46	0.46	0.42	0.47	0.32	0.39
	p-value	*	*	**	**	**	**	**	**	*	*	*	*	**	**	**	**
FL1	Pearson r	1 week	0.59	0.47	0.81	0.85	0.90	0.89	0.78	0.56	0.54	0.45	0.45	0.38	0.44	0.35	0.41
	p-value	*	*	**	**	**	**	**	**	*	*	**	**	**	**	**	**
FL2	Pearson r	1 week	0.63	0.58	0.81	0.80	0.84	0.82	0.82	0.58	0.54	0.48	0.45	0.37	0.45	0.30	0.37
	p-value	*	*	**	**	**	**	**	**	*	*	*	*	**	**	**	**
FL3	Pearson r	1 week	0.61	0.53	0.84	0.84	0.88	0.85	0.84	0.61	0.59	0.50	0.45	0.27	0.42	0.29	0.35
	p-value	*	*	**	**	**	**	**	**	*	*	*	**	**	**	**	**
A	Pearson r	1 week	0.59	0.57	0.64	0.63	0.67	0.70	0.50				0.45	0.50	0.47	0.43	0.49
	p-value	*	*	*	*	*	*	**	*	*	*	*	**	**	**	**	**
B	Pearson r	1 week	0.56										0.39	0.41	0.37	0.23	0.32
	p-value	*	*										**	**	**	**	**
AB	Pearson r	1 week	0.56	0.45	0.74	0.79	0.85	0.86	0.71	0.49	0.48		0.42	0.28	0.44	0.35	0.40
	p-value	*	*	**	**	**	**	**	**	*	*	*	**	**	**	**	**
BC	Pearson r	1 week	0.51						0.53				0.43	0.35	0.39	0.27	0.34
	p-value	*	*						*				**	**	**	**	**
ABC	Pearson r	1 week	0.57		0.83	0.87	0.92	0.89	0.81	0.61	0.60		0.43	0.22	0.38	0.29	0.34
	p-value	*	*	**	**	**	**	**	**	*	*	*	**	**	**	**	**
AB+ABC	Pearson r	1 week	0.60	0.48	0.82	0.86	0.91	0.89	0.79	0.58	0.57		0.43	0.24	0.41	0.32	0.37
	p-value	*	*	**	**	**	**	**	**	*	*	*	**	**	**	**	**

**Table S3.** Pearson correlation analysis. \*: p<0.05, \*\*: p<0.0001



**Figure S12.** High temperature INP concentrations measured with INSEKT.

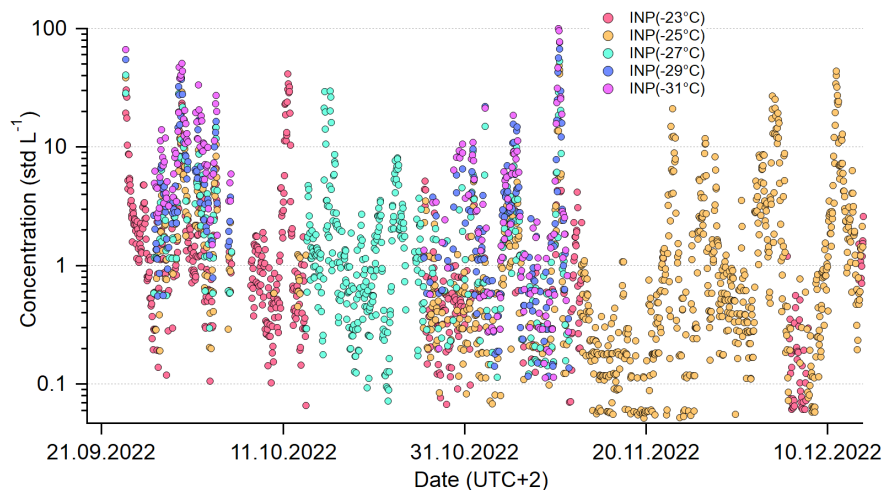


**Figure S13.** Low temperature INP concentrations measured with PINE.

## 8 Impactor measurements

130 In parallel with INP and eDNA filter sampling, a Sioutas Personal Cascade Impactor was used (described in the main text, Section 2). Fluorescent particle concentrations were determined by analyzing stages A and B: ( $Da > 2.5 \mu\text{m}$  and  $1.0 < Da < 2.5 \mu\text{m}$ , respectively). Fluorescent particles were examined using a fluorescence microscope. The impacted area was estimated by measuring its length with a slide gauge and its width at three different positions using microscope software. For each stage, three images of fluorescent particles ( $\lambda_{ex}=465\text{--}495 \text{ nm}$ ,  $\lambda_{ex}=515\text{--}555 \text{ nm}$ ) were taken at approximately the middle, 135 one-quarter, and three-quarters of the impaction area length using a 10x magnification. Fluorescent particles were counted in

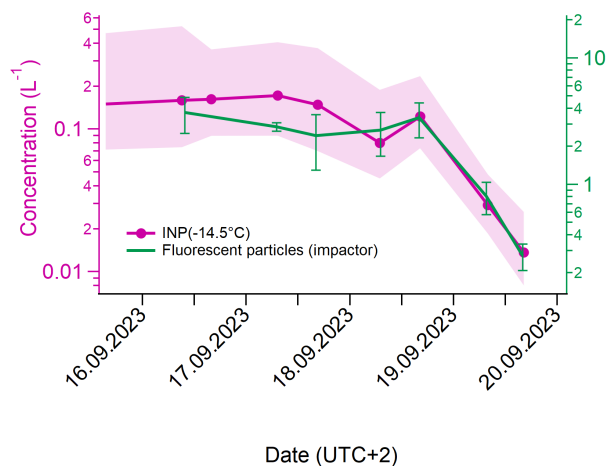


**Figure S14.** INP concentration at -14.5 °C and concentration of fluorescent particles > 1 µm (aerodynamic diameter) impacted on stage A and B on the cascade impactor.

ImageJ after setting an automatic threshold via the triangle method. The image area was then compared to the total impaction area. A mean value and standard deviation were calculated from three measurements per impaction foil. The total number of fluorescent particles >1.0 µm (aerodynamic diameter) was determined by summing particle counts from stages A and B. Concentrations were then calculated by dividing by the air volume passing through the impactor. Concentrations of fluorescent particles were probably underestimated with this method due to bouncing of particles and subsequent impaction on lower stages that were not examined.

The resulting concentration, as well as the concentration of INPs active at -14.5 °C is plotted in Fig. S14. Both concentrations stay relatively constant for 6 measurements (5 for the impactor) before dropping by approximately one order of magnitude during the final two measurements, coinciding with a snow storm. Most of the fluorescent particles examined in detail were identified as fungal spores (see main text sect. 3.6, Fig. 8).

## References

- Abdel Hameed, A., Khoder, M., Yuosra, S., Osman, A., and Ghanem, S.: Diurnal distribution of airborne bacteria and fungi in the atmosphere of Helwan area, Egypt, *Sci Total Environ*, 407, 6217–6222, <https://doi.org/10.1016/j.scitotenv.2009.08.028>, 2009.
- Allitt, U.: Airborne fungal spores and the thunderstorm of 24 June 1994, *Aerobiologia*, 16, 397–406, <https://doi.org/10.1023/A:1026503500730>, 2000.
- Bauer, H., Kasper-Giebl, A., Löflund, M., Giebl, H., Hitzengerger, R., Zibuschka, F., and Puxbaum, H.: The contribution of bacteria and fungal spores to the organic carbon content of cloud water, precipitation and aerosols, *Atmospheric Research*, 64, 109–119, [https://doi.org/10.1016/S0169-8095\(02\)00084-4](https://doi.org/10.1016/S0169-8095(02)00084-4), 2nd International Conference on Fog and Fog Collection, 2002.
- Burrows, S. M., Elbert, W., Lawrence, M. G., and Pöschl, U.: Bacteria in the global atmosphere – Part 1: Review and synthesis of literature data for different ecosystems, *Atmospheric Chemistry and Physics*, 9, 9263–9280, <https://doi.org/10.5194/acp-9-9263-2009>, 2009.
- Crawford, I., Lloyd, G., Herrmann, E., Hoyle, C. R., Bower, K. N., Connolly, P. J., Flynn, M. J., Kaye, P. H., Choularton, T. W., and Gallagher, M. W.: Observations of fluorescent aerosol–cloud interactions in the free troposphere at the High-Altitude Research Station Jungfraujoch, *Atmos Chem Phys*, 16, 2273–2284, <https://doi.org/10.5194/acp-16-2273-2016>, 2016.
- Després, V., Huffman, J. A., Burrows, S. M., Hoose, C., Safatov, A., Buryak, G., Fröhlich-Nowoisky, J., Elbert, W., Andreae, M., Pöschl, U., et al.: Primary biological aerosol particles in the atmosphere: a review, *Tellus B: Chem Phys Meteorol*, 64, 15 598, <https://doi.org/10.3402/tellusb.v64i0.15598>, 2012.
- Flossmann, A. I. and Wobrock, W.: A review of our understanding of the aerosol–cloud interaction from the perspective of a bin resolved cloud scale modelling, *Atmos Res*, 97, 478–497, <https://doi.org/10.1016/j.atmosres.2010.05.008>, from the Lab to Models and Global Observations: Hans R. Pruppacher and Cloud Physics, 2010.
- Gosselin, M. I., Rathnayake, C. M., Crawford, I., Pöhlker, C., Fröhlich-Nowoisky, J., Schmer, B., Després, V. R., Engling, G., Gallagher, M., Stone, E., Pöschl, U., and Huffman, J. A.: Fluorescent bioaerosol particle, molecular tracer, and fungal spore concentrations during dry and rainy periods in a semi-arid forest, *Atmos Chem Phys*, 16, 15 165–15 184, <https://doi.org/10.5194/acp-16-15165-2016>, 2016.
- Gregory, P. H. and Hirst, J. M.: The Summer Air-Spora at Rothamsted in 1952, *Microbiology*, 17, 135–152, <https://doi.org/10.1099/00221287-17-1-135>, 1957.
- Healy, D., Huffman, J., O'Connor, D. J., Pöhlker, C., Pöschl, U., and Sodeau, J.: Ambient measurements of biological aerosol particles near Killarney, Ireland: a comparison between real-time fluorescence and microscopy techniques, *Atmos Chem Phys*, 14, 8055–8069, <https://doi.org/10.5194/acp-14-8055-2014>, 2014.
- Heo, K. J., Kim, H. B., and Lee, B. U.: Concentration of environmental fungal and bacterial bioaerosols during the monsoon season, *J Aerosol Sci*, 77, 31–37, <https://doi.org/10.1016/j.jaerosci.2014.07.001>, 2014.
- Hernandez, M., Perring, A. E., McCabe, K., Kok, G., Granger, G., and Baumgardner, D.: Chamber catalogues of optical and fluorescent signatures distinguish bioaerosol classes, *Atmos Meas Tech*, 9, 3283–3292, <https://doi.org/10.5194/amt-9-3283-2016>, 2016.
- Hill, S. C., Pinnick, R. G., Niles, S., Fell, N. F., Pan, Y.-L., Bottiger, J., Bronk, B. V., Holler, S., and Chang, R. K.: Fluorescence from airborne microparticles: dependence on size, concentration of fluorophores, and illumination intensity, *Appl Opt*, 40, 3005–3013, <https://doi.org/10.1364/ao.40.003005>, 2001.
- Hirst, J. M. and Stedman, O. J.: Dry Liberation of Fungus Spores by Raindrops, *Microbiology*, 33, 335–344, <https://doi.org/10.1099/00221287-33-2-335>, 1963.

- Huffman, J. A., Prenni, A., DeMott, P., Pöhlker, C., Mason, R., Robinson, N., Fröhlich-Nowoisky, J., Tobo, Y., Després, V., Garcia, E., et al.: High concentrations of biological aerosol particles and ice nuclei during and after rain, *Atmos Chem Phys*, 13, 6151–6164, <https://doi.org/10.5194/acp-13-6151-2013>, 2013.
- 185 Lighthart, B. and Shaffer, B. T.: Airborne Bacteria in the Atmospheric Surface Layer: Temporal Distribution above a Grass Seed Field, *Appl Environ Microbiol*, 61, 1492–1496, <https://doi.org/10.1128/aem.61.4.1492-1496.1995>, 1995.
- Prenni, A., Tobo, Y., Garcia, E., DeMott, P., Huffman, J., McCluskey, C., Kreidenweis, S., Prenni, J., Pöhlker, C., and Pöschl, U.: The impact of rain on ice nuclei populations at a forested site in Colorado, *Geophys Res Lett*, 40, 227–231, <https://doi.org/10.1029/2012GL053953>, 2013.
- 190 Rathnayake, C. M., Metwali, N., Jayarathne, T., Kettler, J., Huang, Y., Thorne, P. S., O’Shaughnessy, P. T., and Stone, E. A.: Influence of rain on the abundance of bioaerosols in fine and coarse particles, *Atmos Chem Phys*, 17, 2459–2475, <https://doi.org/10.5194/acp-17-2459-2017>, 2017.
- Savage, N. J., Krentz, C. E., Könemann, T., Han, T. T., Mainelis, G., Pöhlker, C., and Huffman, J. A.: Systematic characterization and fluorescence threshold strategies for the wideband integrated bioaerosol sensor (WIBS) using size-resolved biological and interfering particles, *Atmos Meas Tech*, 10, 4279–4302, <https://doi.org/10.5194/amt-10-4279-2017>, 2017.
- 195 Schumacher, C., Pöhlker, C., Aalto, P., Hiltunen, V., Petäjä, T., Kulmala, M., Pöschl, U., and Huffman, J.: Seasonal cycles of fluorescent biological aerosol particles in boreal and semi-arid forests of Finland and Colorado, *Atmos Chem Phys*, 13, 11 987–12 001, <https://doi.org/10.5194/acp-13-11987-2013>, 2013.
- Sellegri, K., Laj, P., Dupuy, R., Legrand, M., Preunkert, S., and Putaud, J.-P.: Size-dependent scavenging efficiencies of multicomponent atmospheric aerosols in clouds, *J Geophys Res: Atmos*, 108, <https://doi.org/10.1029/2002JD002749>, 2003.
- 200 Yue, S., Ren, H., Fan, S., Sun, Y., Wang, Z., and Fu, P.: Springtime precipitation effects on the abundance of fluorescent biological aerosol particles and HULIS in Beijing, *Sci Rep*, 6, 29 618, <https://doi.org/10.1038/srep29618>, 2016.
- Šantl Temkiv, T., Živec, M., Lund, M. B., Benčina, M., Bohn, A. B., Stanič, S., and Močnik, G.: The limited capacity of bioaerosols to serve as cloud-condensation nuclei may restrict their potential to initiate ice formation in mixed-phase clouds, *bioRxiv*, p. 2024.10.30.621021, <https://doi.org/10.1101/2024.10.30.621021>, 2024.
- 205